Particle Accelerators, 1987, Vol. 22, pp. 161–175
Photocopying permitted by license only

Printed in the United States of America

EXPERIMENTS WITH AN RFQ SPARKER

R. LEHMANN
ASI, Kernforschungsanlage Jülich, Postfach 1913, D-5170 Jülich, West Germany

(Received August 28, 1986; in final form November 26, 1986)

Design, manufacture, and rf adjustment procedures of a prototype 100-MHz radio-frequency quadrupole cavity are described, along with some results of experiments made without a beam. The rf voltage amplitude at the electrodes was measured via the upper edge of the x-ray spectrum. A much simpler method for measuring the rf voltage with 4% accuracy was established by evaluating the dependence of the x-ray intensity on iron shield thickness and voltage; the first method was used to calibrate the second. The voltage dependence of the electron current emitted by the electrodes was computed from measured x-ray dose rates and was compared with the Fowler-Nordheim theory of field emission. Finally, the breakdown behavior at high field strengths up to 30 MV/m is described; it was found that the breakdown threshold depends on the pulse length, as well as on previous conditioning or deconditioning, and is approximately 2.5 times the Kilpatrick limit.

1. INTRODUCTION

As a preaccelerator for a spallation neutron source,[1,2] two identical radio-frequency quadrupoles (RFQs)[3] have been proposed. The operating frequency is 100.625 MHz; the particle bunches from the two RFQs were to be funneled together[2,4] and further accelerated in a drift tube linac at twice the frequency. A prototype[5] (RFQ2) of the RFQs is being manufactured and will not be described here. An rf cavity, RFQ1 ("RFQ sparker"), was constructed in order to study the machining of the pole tips, rf adjustment procedures, the measurement of the pole-tip voltage, and the breakdown behavior of RFQ2.

2. DESCRIPTION OF RFQ1

The inner cross section (see Fig. 1) and the resonant frequency of the four-vane resonator[3] of RFQ1 were chosen identical to those of RFQ2. The resonant frequency of the TE_{210} mode utilized here does not depend on the length of the cavity. For a constant cross section, the resonant frequency and field distributions can be computed as a two-dimensional problem, assuming infinite length with the program SUPERFISH.[6] For the stabilization of the azimuthal field distribution, the cavity has two vane coupling rings (VCRs),[3,7] which constitute a capacitive load shifting the resonant frequency down by 5%. This three-dimensional problem was reduced to two dimensions as follows: First, a geometry having a resonant frequency 5% higher than the operating frequency was found by using SUPERFISH in a trial-and-error procedure. Then, the influence of the VCRs was approximately simulated by lowering the aperture radius in the SUPERFISH

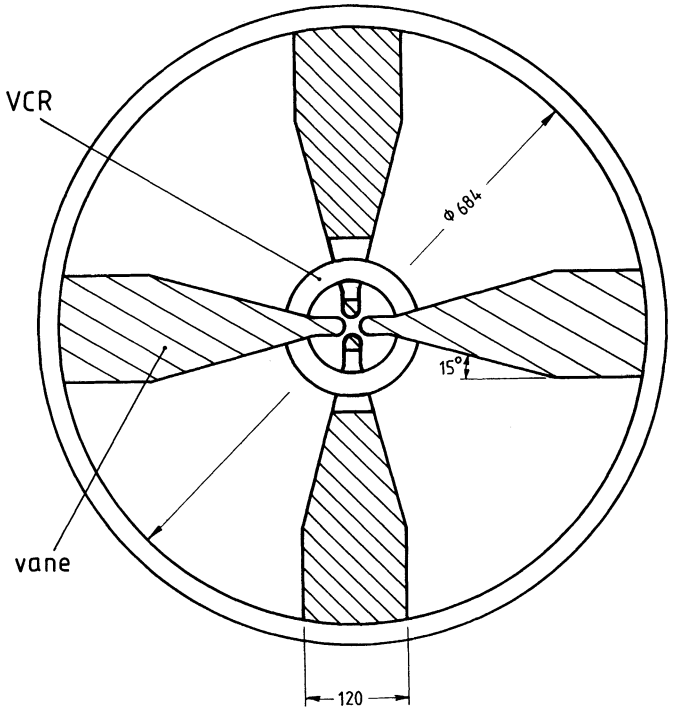

FIGURE 1 Cross section of RFQ1. Dimensions are in millimeters.

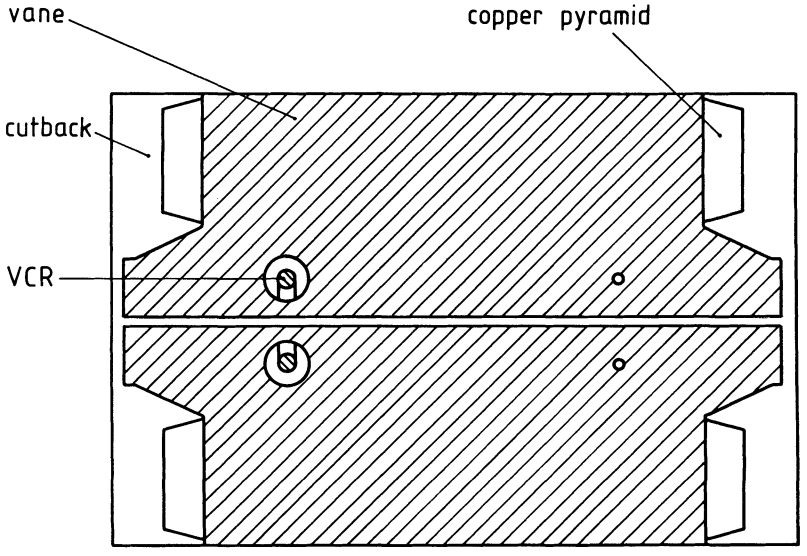

FIGURE 2 Longitudinal section of RFQ1.

computation such that the resonant frequency was 100.6 MHz. The theoretical quality factor and equivalent parallel resistance were 19,300 and 235 kΩ, respectively. Values this high cannot be expected in reality, because they do not account for the effects of pumping slots, orifices, VCRs, and tank ends, all of which make the current distribution inhomogeneous, thus increasing the power loss. In order to allow the magnetic field lines to return, the vanes have to have cutbacks at their ends, as shown in Fig. 2.

The length of RFQ1 is one meter, that is, only one-third the length of RFQ2. The pole tips are modulated; the profile is identical to that of a section of RFQ2 located 0.5 to 1.5 m from its front end. The modulation could not be simulated in the SUPERFISH calculation. The section chosen contains those accelerating and bunching cells of RFQ2 in which the greatest electrical field strength is expected.[8] The characteristic aperture radius[8] r_0 equals 1.3 cm; the transverse radius of curvature is kept constant at 1.0 cm. The minimum gap between the poles is approximately 1.1 cm. The maximum surface field strength is not known exactly; it was assumed to be $E = 1.36\, U_p/r_0$.

In contrast to RFQ2, no cooling and no piston tuners are present in RFQ1. When detuning occurred (lowering of the resonant frequency during operation due to warm-up), the operating frequency was changed correspondingly.

The tank cylinder and end plates were manufactured out of mild steel, the vanes out of aluminium. All inner surfaces were plated with a 5-μm base layer of nickel and 50 μm of copper. The oxide layer on the aluminium vanes was removed by an acid bath prior to nickel plating. The thickness of the vane plating

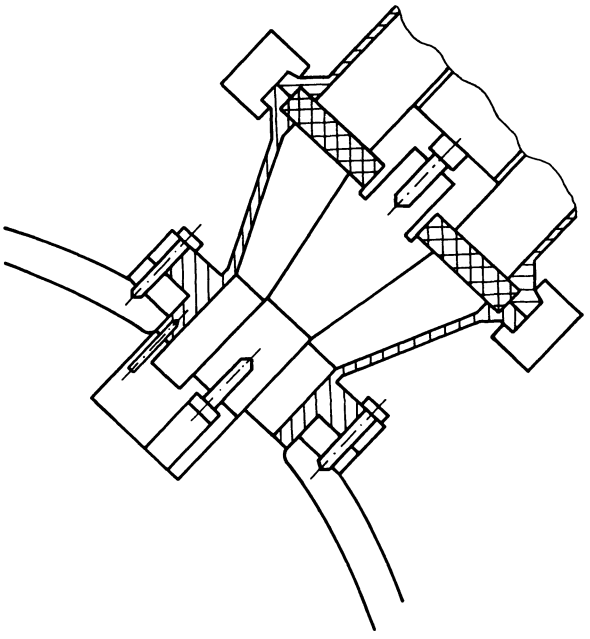

FIGURE 3 Cross section of the rf vacuum feedthrough ("rf window").

was measured mechanically, as the usual technique requires a magnetic substrate. The surface roughness is less than a micrometer, i.e., much less than the skin depth of 7 μm. As vacuum seals, aluminum wires (at flanges and end plates) and Viton O-rings (at vane bases) were used. Although there are cavities under the vanes constituting "virtual leaks", a pressure of 10^{-7} mbar was achieved with a 1000 l/s turbomolecular pump. Rf contact between vane bases and tank was achieved by silver-plated Cu-Be canted helical springs.

Shims were used under the vane bases in order to position the pole tips within 0.2 mm, relative to each other.

Each end plate has three glass windows for inspections and radiation measurements.

Rf power was fed into RFQ1 via a rigid $3\frac{1}{8}$-inch coaxial line from a 1.2-MW power amplifier. A coaxial rf vacuum feedthrough (Fig. 3) was constructed; at its vacuum end, rf power is fed into the cavity inductively by a loop in one quadrant. The insulating disk is made of Teflon and could as well be of polyethylene; all inner dimensions of the feedthrough were chosen such that the characteristic impedance equals 50 Ω if the relative dielectric constant of the disk equals 2.3. Vacuum sealing is achieved through sharp edges cutting into the disk.

Two diagnostic loops provide signals proportional to the rf voltage in the cavity; they are situated on the air side of glass cups on the tank wall in two different quadrants (Fig. 4).

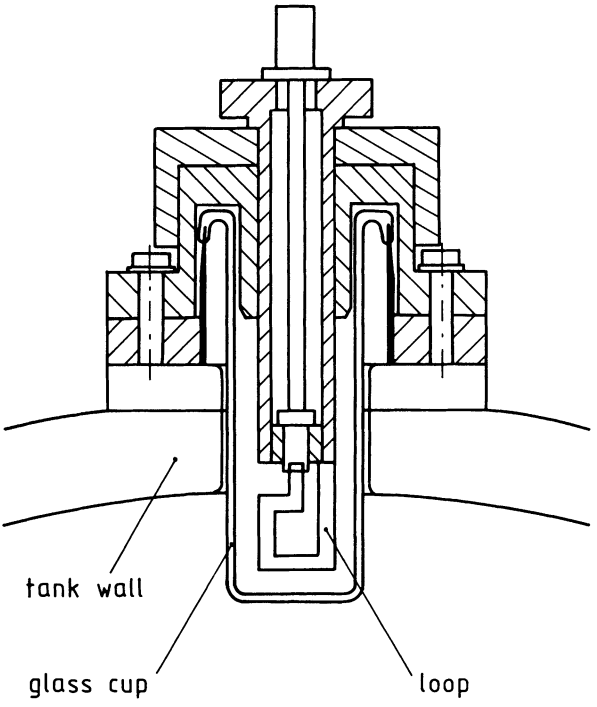

FIGURE 4 Diagnostic loop.

3. RF ADJUSTMENTS

3.1. Longitudinal Voltage Distribution

The voltage between adjacent pole tips should be distributed uniformly over the length. The voltage distribution was measured using the perturbation method:[9] A dielectric cube was pulled with a thread along the outer sides of an arbitrary pair of pole tips, touching both of them. The shift of the resonant frequency is proportional to the electric field energy in the volume of the perturbator. The author assumed the frequency shift to be proportional to the square of the pole-tip voltage in places, where the field distribution is not perturbed by a VCR or a vane end.

Deviations from a uniform distribution are, in particular, due to (i) wrong size of the vane cut-backs and (ii) nonuniform distribution of the pole-tip capacitance. The area of the cut-backs was adjusted by successively milling off portions of eight pyramid-shaped copper bodies (shown in Fig. 2) until the voltages measured at the ends and in the middle agreed with each other within measurement accuracy, which was approximately 4%.

An essential variation of the voltage due to the variation of the pole-tip modulation was not observed; however, the capacitance of the VCRs cause a local voltage hump of 1.4%. These voltage humps could have been avoided by placing the two VCRs at the vane ends; RFQ1 was, however, a model for RFQ2, which has six VCRs, spaced uniformly in order to minimize the magnitude of the voltage humps.

3.2. Transverse Voltage Distribution

The four quadrant voltages agreed with each other, as they should, within measurement accuracy in every cross section, without any adjustment; this is due to the VCRs.

3.3. Feeder Loop

The size of the feeder loop should be chosen such that the equivalent parallel resistance of the cavity is transformed to the characteristic impedance of the feeder line; otherwise, a considerable portion of the rf power is reflected to the amplifier. The magnitude and phase of the reflection coefficient of the feeder loop were measured with a network analyzer, and the loop area was modified by milling off portions until the magnitude of the reflection coefficient was less than 5% for one frequency.

During the first high-power operation, multipactoring[10] was observed with the cavity voltage breaking down to 10% and with light shining from the vacuum side of the feedthrough. Therefore, the inner sides of the loop and the coaxial metal parts on the vacuum side were coated with an aquadag graphite layer, whose

secondary electron emission yield is small.[11] The aquadag's liquid was isopropanol, which is not hygroscopic. The carbon layer hides the metal surfaces, although it is only a few micrometers thick. It is smooth and adheres rather well—only three or four particles of about 0.5 mm diameter broke off during operation. No multipactoring and no other adverse effects were observed after the coating.

4. MEASUREMENT OF THE X-RAY SPECTRUM

Because there is no cooling, RFQ1 was operated in a pulsed mode; typical pulse data were: pulse duration = 300 μs, repetition rate = 20 Hz, pulse power = 100 kW, amplitude of pole-tip voltage = 170 kV. As the pole tips are not accessible for a direct rf voltage measurement, the amplitude was measured indirectly via x-rays. This method has been previously described for cw operation by Hutcheon *et al.*[12] Electrons are field emitted from a pole tip and accelerated by the rf voltage; when they hit the adjacent pole, their energy corresponds to the instantaneous value of the rf voltage, as their run time is small compared with the rf period. Therefore, the high-energy edge of their x-ray (Bremsstrahlung) spectrum corresponds to the amplitude of the rf voltage. The spectrum was measured with a high-purity germanium detector and a multichannel analyzer. RFQ1 had a shielding of 4 mm of lead; only radiation out of the glass window in the center of an end wall was allowed to come through an orifice in the shielding and was measured.

If too much radiation hits the dectector, pileup occurs: Two or more photons

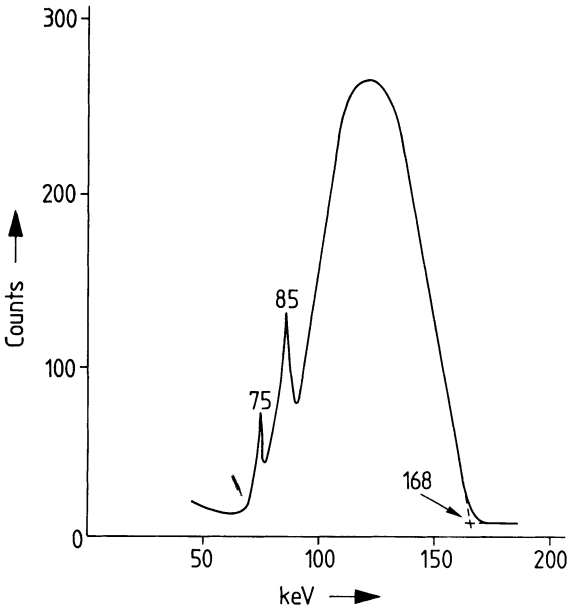

FIGURE 5 Typical x-ray spectrum.

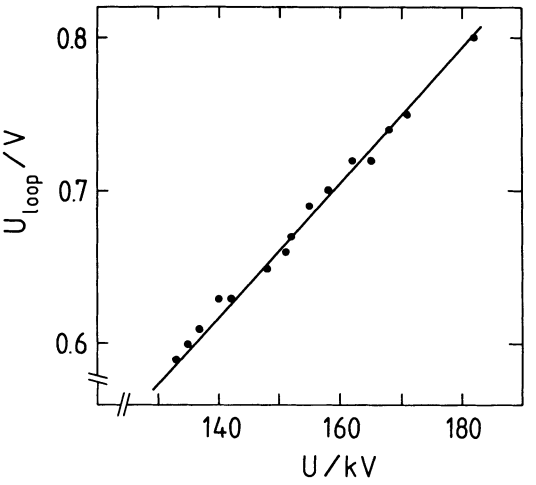

FIGURE 6 Rf voltage at diagnostic loop vs electrode voltage.

are not discriminated and are counted as one photon, the energy of which is close to the sum of the energies of the actual photons. In order to avoid excessive pileup, the detector received a lead shielding with a small hole, and low-energy radiation was attenuated by several millimeters of steel. The distance of the detector from RFQ1 was varied in order to vary the count rate. Total (i.e., energies from a few to a few hundred keV) rates of 10,000 to 60,000 counts in five minutes yielded satisfactory spectra.

Figure 5 shows a typical spectrum. The peaks at approximately 75 and 85 keV are k_α and k_β radiation of lead (electrons excited by primary radiation fall from L and M shells back to the K shell, emitting characteristic x-rays). The detector was calibrated with a radioactive x-ray emitter.

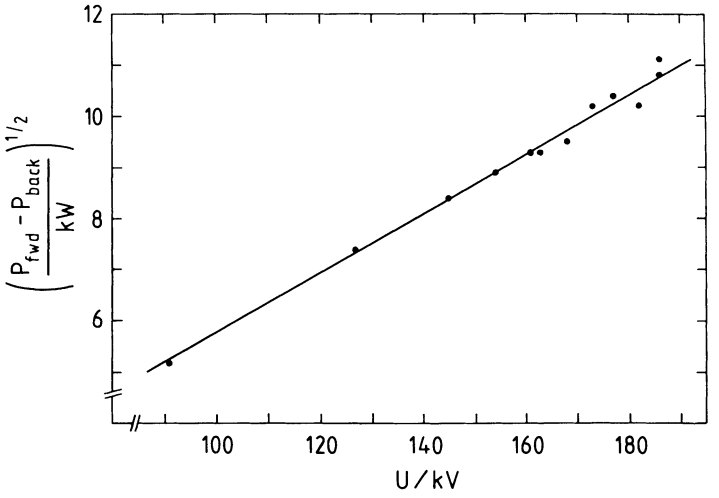

FIGURE 7 Square root of rf power in cavity vs electrode voltage.

Figures 6 and 7 show measured values of the amplitude at a diagnostic loop and of the rf power in the cavity, measured with directional couplers in the feeder line (forward minus backward power), versus the rf voltage (edge of spectrum). The equivalent parallel resistance turned out to be 150 kΩ, that is, 64% of the theoretical value of 235 kΩ.

The accuracy of this voltage measurement method is approximately 1–2%. A series of measurements, where the radiation was measured in different places on the side with a collimator (without the RFQ1 shielding) did not discriminate the voltage peaks at the VCRs, expected to be 1.4% of the average voltage.

5. AN ALTERNATIVE VOLTAGE MEASUREMENT METHOD

In order to have at our disposal a much simpler and faster method for measuring the electrode voltage with sufficient accuracy, a method employing an ionization chamber radiation meter was calibrated with the x-ray edge method. Figure 8 shows the measured x-ray intensity 5 cm from the orifice in the RFQ1 shielding, versus the thickness d of a steel shielding for different voltages. The slope of the straight portions (in the half logarithmic representation) of the curves is a function of the voltage. These slopes were evaluated with least-squares fits and are represented in Fig. 9 as tenth-value thickness $d_{10,\mathrm{Fe}}$ versus the voltage. This

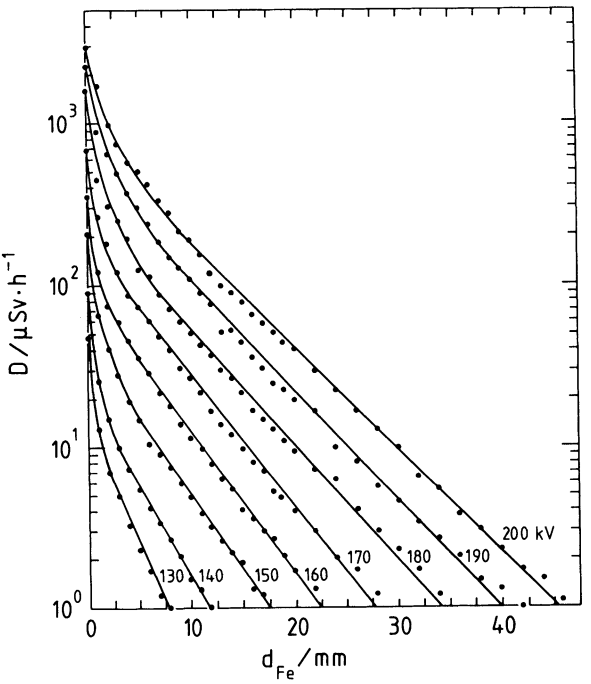

FIGURE 8 Dependence of x-ray dose rate on iron shield thickness and electrode voltage; 1 Sv = 1 Sievert = 1 "Gray equivalent man" = 100 rem.

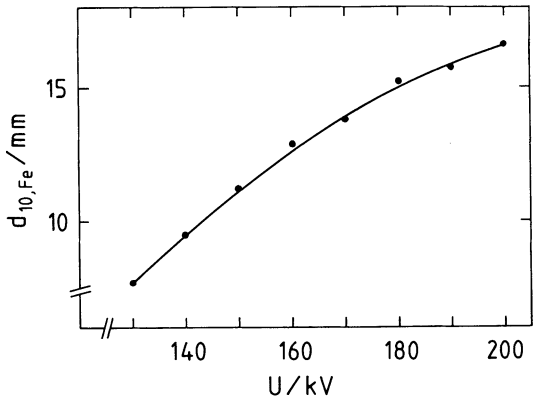

FIGURE 9 Tenth-value iron thickness vs voltage amplitude.

curve is valid only if there is a basic steel shielding of the thickness d_0 providing a shielding factor of about 20.

Measuring in a simple transmission experiment the x-ray dose rates $D(d_0)$, with the basic shielding, and $D(d_0 + x)$, with an additional shielding of the thickness x, the tenth-value thickness is

$$d_{10} = x/\log_{10} y, \tag{1}$$

where $y = D(d_0)/D(d_0 + x)$. Using the calibration curve (Fig. 9), one is able to determine the voltage U.

There are two sources of error in the determination of U. The first is the inaccuracy of the calibration curve of approximately

$$(dU/U)_1 = 2\%, \tag{2}$$

which must be added in an rms sense to the inaccuracy due to the error of the dose-rate ratio measurement. For $y = 10$ and $U = 170\,\text{kV}$, this inaccuracy is fortunately only one-third of the ratio error:

$$(dU/U)_2 = 0.33\, dy/y. \tag{3}$$

Specifications and calibration data of the ionization chamber used for our measurements revealed that dose-rate ratios are measured with an error of 9%. Equations (2) and (3) and

$$(dU/U)^2 = (dU/U)_1^2 + (dU/U)_2^2 \tag{4}$$

result in an overall error of some 4%.

In order to improve the accuracy, one can make several measurements with different steel thicknesses and compute d_{10} via a least-squares fit.

Either of the two methods described here is more accurate than the usual method of calculating the voltage from rf power and parallel resistance. The latter could not be determined exactly from SUPERFISH calculation and Q measurements because of the effect of the tank ends. Moreover, the author's rf

equipment allowed the determination of rf power only with an accuracy of some 5%.

6. ELECTRON POWER

The electron power was determined because the author was curious to know (i) the portion of rf power lost by field emission and (ii) the electron current available for possible future experiments. The dose-rate constant $G(U)$ is defined as

$$G = D_p r^2 / I, \tag{5}$$

where I is the dc electron current and D_p is the dose rate measured at a distance r from a point source. If the dose rate is measured on the axis of a line source of length l at a distance d from its end, then r^2 is to be replaced by $d(d+l)$. G is given, for example, in Refs. 13 and 14 as a function of the (dc) voltage and the thickness and material of different radiological filters.

Approximating the four pole tips by a single line source and assuming the dose-rate constant at an ac voltage with the amplitude U to be equal to the dose-rate constant at a dc voltage U, the "equivalent dc current" is

$$I = d(d+l)D/G(U), \tag{6}$$

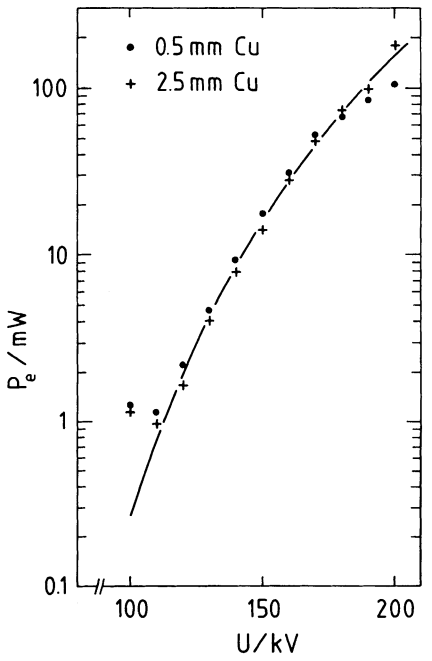

FIGURE 10 Electron power vs voltage amplitude.

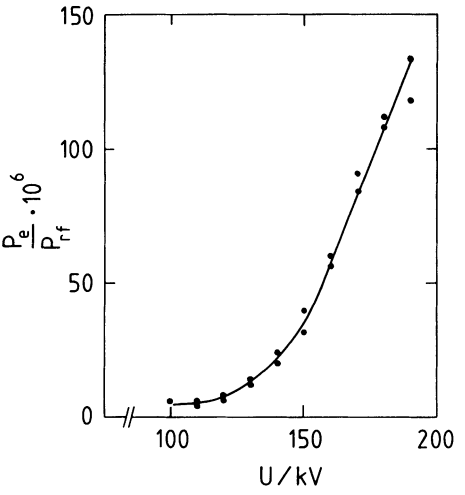

FIGURE 11 Voltage dependence of rf – to – electron power conversion ratio.

and the electron power is

$$P_e = UI = Ud(d + l)D/G(U). \tag{7}$$

Measurements were made with an ionization chamber and copper filters 0.5 and 2.5 mm thick at different voltages; the electron powers from these measurements and Eq. (7) are shown as points in Fig. 10.

The theory of field emission (Fowler and Nordheim) gives[15]

$$P_e = c_1 U^3 \exp(-c_2/U). \tag{8}$$

The constants are not known a priori, because they are functions of the electric field enhancement factor and the electron work function and thus are influenced by the presence of microscopic tips, edges, and contaminations on the pole surfaces. The curve in Fig. 10 results from a fit of Eq. (8) to measured points; the constants are $c_1 = 1.4\,\mu\text{W MV}^{-3}$ and $c_2 = 855\,\text{kV}$. Assuming ideally smooth and clean pure copper surfaces, the Fowler-Nordheim formula leads to a value for c_2 three orders of magnitude larger. This clearly demonstrates that the behavior of the emitted current is governed by surface imperfections.

The portion of the (time-averaged) rf power transformed into electron power turned out to be very small and is shown versus the voltage in Fig. 11.

7. CONSIDERATION OF THE RF TIME FUNCTION

In the previous section, a simplification was made: Electrons were assumed to be emitted only when the momentary value of the voltage is equal to the positive or negative amplitude. Under this assumption, the "equivalent current" I can be regarded as the time average of the electron current. In this section, an investigation will be made on the quality of the above assumptions.

Equation (8) was used as a first approximation for the dependence of the instantaneous electron current on the instantaneous value U of the voltage:

$$I(U) = cU^2 \exp(-855/U), \tag{9}$$

with the time function ($\varphi = \omega t$)

$$U(\varphi) = U_p \sin \varphi. \tag{10}$$

The probability function of the current can then be computed as

$$F_I(\varphi) = \int_0^{\varphi} I[U(\varphi)]\, d\varphi \Big/ \int_0^{\pi/2} I[U(\varphi)]\, d\varphi. \tag{11}$$

Taking into account Eq. (10), the probability function $F_I(U)$ was computed and is shown for $U_P = 170$ kV in Fig. 12. One can, for example, read from Fig. 12 that 90% of all electrons are accelerated to at least 84% of the amplitude of the voltage.

A different quantity might, however, be of greater interest, namely, the probability function of the radiation with respect to the voltage, $F_x(U)$. In one computation, it was assumed that the radiation intensity D is proportional to the x-ray power P_x; the x-ray efficiency P_x/P_e is, to a good approximation, proportional to the voltage.[16] With Eq. (9), one gets

$$D = cU^4 \exp(-855/U). \tag{12}$$

The tabulated values of $G(U)$ can be approximated in the range 100–200 kV by

$$G = cU(U - U_0), \tag{13}$$

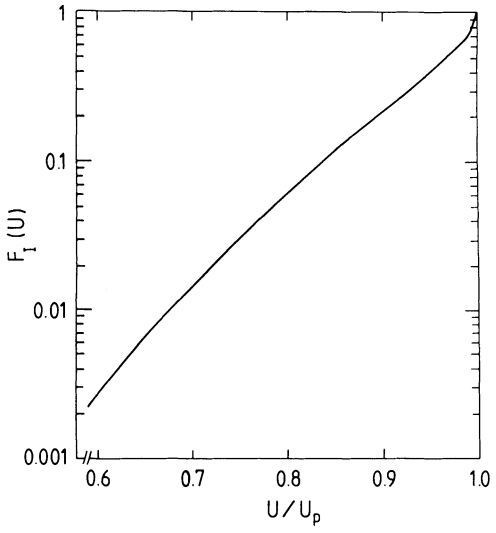

FIGURE 12 Probability function of the electron current; $U_p = 170$ kV.

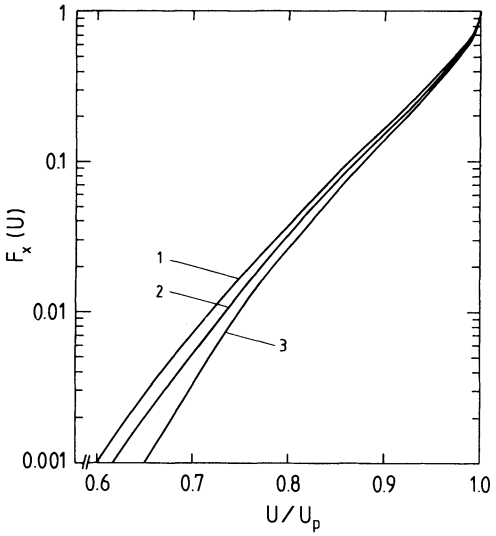

FIGURE 13 Probability function of x-ray dose rate; $U_p = 170$ kV. Curve 1, no filter; 2, copper filter, 0.5 mm; 3, copper filter, 2.5 mm.

with

$$U_0 = 60 \text{ kV at } d_{Cu} = 0.5 \text{ mm},$$
$$U_0 = 90 \text{ kV at } d_{Cu} = 2.5 \text{ mm}.$$

Thus, with filtering one gets

$$D = c(U - U_0)U^3 \exp(-855/U). \tag{14}$$

The probability function

$$F_x(\varphi) = \frac{\int_0^{\varphi} D[U(\varphi)]\, d\varphi}{\int_0^{\pi/2} D[U(\varphi)]\, d\varphi} \tag{15}$$

was computed using Eqs. (12) and (14) respectively. Transformation using Eq. (10) and $U_p = 170$ kV resulted in the functions $F_x(U)$ shown in Fig. 13. From this figure, one can, for example, get the information that at $d_{Cu} = 2.5$ mm 90% of the radiation was generated by at least 88% of the rf amplitude.

Figures 12 and 13 allow the conclusion that electron current and x-rays occur essentially only if the instantaneous value of the voltage is close to its amplitude.

8. BREAKDOWN BEHAVIOR

Rf breakdown and sparking is very little understood. There is an empirical criterion[17] that gives an electric field strength threshold ("Kilpatrick limit"),

below which no breakdowns occur. This threshold is 11.4 MV/m for RFQ1, corresponding to 110 kV. This is far below the observed thresholds.

Sparks were counted during pulsed operation by a universal counter, which compared the number of breakdowns of the rf amplitude at an outcoupling loop with the number of rf pulses. The rf drive was not cut off upon the detection of a spark. Each spark dissipated all or most of the energy stored in the cavity (approximately 4.5 J at 270 kV). The vacuum pressure varied from 10^{-7} mbar (no rf for days) to 10^{-5} mbar (several sparks per second); usually, the pressure was about 10^{-6} mbar during sparking experiments.

Most of the breakdowns could only be observed by looking at the rf amplitude; only a few of them were accompanied by blue light flashes, which were observed through one of the glass windows with a mirror (to avoid radiation hazard).

No sparks were observed at less than 250 kV; when the voltage was increased to 280 kV, the spark rate increased faster than linearly with the voltage, reaching approximately six sparks per 1000 rf pulses. Then the voltage was lowered, until no more breakdowns occurred. Evidently the sparks had conditioned the surfaces, for the threshold was now 265 kV. Going up to 295 kV and six sparks per 1000 pulses raised the threshold to 280 kV. The threshold could not be increased further; on the contrary, further experiments with spark rates in excess of one spark per 1000 pulses occasionally lowered the threshold (deconditioning). Generally, it can be stated that the sparking behavior is not reproducible at high spark rates. The tendency is that the threshold is higher at shorter pulses and/or lower pulse repetition rates.

In order to get reproducible results, the spark rates were kept at less than two sparks per 1000 pulses in another series of experiments. The pulse length and repetition rate were varied from 150 to 600 μs and from 10 to 40 Hz, respectively. The criterion for the spark threshold was now chosen to be a rate of one spark per 1000 pulses. The threshold voltage was now independent of the repetition rate. The dependence on the pulse length is given in Table I. The rise time of the rf amplitude (included in the pulse length) was approximately 50 μs.

In order to find out whether or not rf and sparking remove the adsorbates on large areas of the pole tips, considerable quantities of ammonia (NH_3) were let in. The threshold voltage and the x-ray intensity did not change. As ammonia adhering on a copper surface is known to lower the work function, it can be concluded that RFQ1's surface is at any time densely covered with adsorbates and thus does not accept the ammonia.

TABLE I

Breakdown Thresholds vs Pulse Length

Pulse Length (μs)	U, threshold (kV)	E, threshold (MV/m)	Kilpatrick factor, E/E(Kilpatrick)
150	295	30.6	2.7
300	272	28.2	2.5
600	254	26.3	2.3

After the sparking experiments, the cavity was opened and inspected. One spark crater (diameter 1.5 mm) exposing the aluminium substrate was found on the side of a pole tip. There was very little copper dust (particles up to 0.1 mm) distributed in the cavity.

ACKNOWLEDGMENTS

The author thanks Dr. J. Schelten for discussions of this work, Mr. W. Klein and his group for careful design and manufacturing, Mr. F. J. Schroeteler and B. Lanz for setup, maintenance, and modifications of RFQ1, an the SNQ rf group for furnishing power amplifiers and rf equipment. This work was done within the framework of the SNQ design at KFA.

REFERENCES

1. *SNQ Project Proposal,* (KFA, 1984).
2. C. Zettler, in *Proc.* 1984 *Linear Accelerator Conf.* (GSI-84-11), p. 480.
3. H. Klein, *IEEE Trans. Nucl. Sci.* **NS-30,** 3313 (1983).
4. K. Bongardt, in *Proc.* 1984 *Linear Accelerator Conf.* (GSI-84-11), p. 389.
5. R. Lehmann, in *Proc.* 1984 *Linear Accelerator Conf.* (GSI-84-11), p. 335.
6. K. Halbach and R. F. Holsinger, *Particle Accelerators* **7,** 213 (1976).
7. H. R. Schneider and H. Lancaster, *IEEE Trans. Nucl. Sci.* **NS-30,** 3007 (1983).
8. K. R. Crandall, R. S. Mills and T. P. Wangler, *IEEE Trans. Nucl. Sci.* **NS-30,** 3554 (1983).
9. L. C. Maier and J. C. Slater. J. Appl. Phys. **23,** 68 (1952).
10. W. J. Gallagher, *IEEE Trans. Nucl. Sci.* **NS-26,** 4280 (1979).
11. *CRC Handbook of Chemistry and Physics,* 65th ed. (CRC Press, Boca Raton, 1985), p. E-352.
12. R. M. Hutcheon *et al.*, *Proc.* 1984 *Linear Accelerator Conf.* (GSI-84-11), p. 74.
13. *DIN* 54113, Teil **3** (Beuth Verlag, Berlin, 1980).
14. M. von Ardenne, *Tabellen zur Angewandten Physik* (VEB Deutscher Verlag der Wissenschaften, Berlin, 1962), Vol. 1, p. 175.
15. S. Flügge, Ed., *Encyclopedia of Physics* (Springer Verlag, Berlin-Göttingen-Heidelberg, 1957), vol. XXX, p. 25.
16. Ref. 14, p. 13.
17. W. D. Kilpatrick, *Rev. Sci. Instrum.* **28,** 824 (1957).